

Intercell Interference Coordination for the ePDCCH in LTE-Advanced Macrocellular Deployments

David González G, Mario Garcia-Lozano, Silvia Ruiz Boqué
 Escola d'Enginyeria de Telecomunicació i Aeroespacial (EETAC)
 Universitat Politècnica de Catalunya
 Barcelona, Spain
 Emails: david.gonzalez.g@ieee.org, {mariogarcia, silvia}@tsc.upc.edu.

Abstract—This paper investigates several schemes to improve the performance of the enhanced Physical Downlink Control Channel (ePDCCH) in Long Term Evolution Advanced (LTE-A) networks by means of Intercell Interference Coordination (ICIC). Given the flexible design of the ePDCCH, based on frequency division multiplexing, static ICIC techniques such as Soft Frequency Reuse (SFR) can be applied and hence, performance degradations at cell edges can be avoided in contrast to its antecesor, the Physical Downlink Control Channel (PDCCH) in LTE. The study is focused in realistic/irregular deployments, where the amount of intercell interference received at different cells varies considerably making very difficult the task of homogenizing the performance of the ePDCCH over the coverage area. In order to address this problem, the proposed multiobjective scheme adjusts the configuration of SFR at cell level. The problem formulation includes several performance metrics including spectral efficiency, cell edge performance, consumption/amount of control resources and energy requirements. The results reveal that the proposed scheme is able to (1) reduce the average consumption of control resources and, (2) minimize energy needs without penalizing the capacity of data channels.

Index Terms—Long Term Evolution Advanced; LTE-A; Soft Frequency Reuse; SFR; Enhanced Physical Downlink Control Channel; ePDCCH; Multiobjective Optimization

I. INTRODUCTION

According to the conclusions in [1], the mobile Internet mass market becomes a reality. The findings of this survey indicate that a tremendous number of Internet users do it through mobile devices, a 69%, from which 61% use smartphones. Mobile operators have answered to this challenge by investing on promising technologies such as Long Term Evolution (LTE) and its evolution, LTE-Advanced (LTE-A) [2]. Indeed, reliable studies forecast 234 commercial LTE networks in 83 countries by the end of 2013 [3].

In this context, it is expected that significant efforts are being placed on LTE-A, the system called to fulfill the expectations of users and industry in the medium term. LTE-A features an interesting set of novelties with respect to LTE such as wider bandwidths, enhanced downlink and uplink transmission, relaying, support of heterogeneous networks and Machine-Type communications among others [2]. However, all these innovations require reliable means to convey an increasing amount of control information. Thus, in 3GPP Release 11, the need for enhanced capabilities for the Physical Downlink Control Channel (PDCCH) was identified [4]. To be

precise, the design of the PDCCH in LTE is much less flexible than the one in data channels. The structure and operation of the PDCCH is described in [5], but basically, there do not exist mechanisms to perform neither frequency domain scheduling nor Intercell Interference Coordination (ICIC) over the PDCCH and hence, low Signal to Interference plus Noise Ratio (SINR) levels at cell edges, a well know issue in Orthogonal Frequency Division Multiple Access (OFDMA), degrade the performance of the PDCCH. Since the control information carried by the PDCCH is highly sensitive, LTE defines some mechanisms to guarantee the required reliability. The most important one is based on Aggregation Levels (ALs), which consists in grouping several Control Channel Elements (CCEs), the basic control information unit, in order to transmit the PDCCH using more robust transmission formats, i.e., lower coding rates. However, higher ALs increase the consumption of CCEs, thus reducing the capacity of the PDCCH. This situation is critical in scenarios with a large number of users using low-rate services such as VoIP as they tend to heavily load the PDCCH. This issue has been analyzed in [6] and [7].

LTE-A provides alternative protection mechanisms for the PDCCH: carrier aggregation plus cross carrier scheduling [8] in the frequency domain and Almost Blank Subframes (ABSs) [9] in the time domain. However, while cross carrier scheduling is not an option for legacy users, ABSs severely penalizes the capacity and hence, its usage has been reserved for Heterogeneous Networks (HetNets). Thus, in the light of these observations, a new enhanced PDCCH (ePDCCH) was introduced in the Release 11 [10]. The ePDCCH employs Frequency Division Multiplexing (FDM) and hence, it allows frequency domain ICIC. In addition, it is compatible with legacy carriers providing more signaling capacity and it can operate in Multicast-Broadcast Single Frequency Network (MBSFN) subframes [11].

However, given its recent appearance (Release 11, 2012), few studies about the ePDCCH have been reported. Indeed, most of the work done about the ePDCCH has been focused on comparing the performance of its baseline design against the conventional PDCCH. The study presented by Einhaus et al. [12] demonstrates that the ePDCCH outperforms the PDCCH in terms of achievable SINR levels mainly due to its inherent capability to perform frequency domain resource allocation. The work presented by Yi et al. [13] is concentrated on the

design of the search space, i.e., how to allocate the enhanced CCEs (eCCEs) [10], the basic control information unit defined for the ePDCCH, in the physical resources devoted for such purpose. Other related works, such as [8] and [9], as indicated before, are just focused on the mechanisms introduced in the Release 10 such as cross carrier scheduling and ABS. To the best of the authors' knowledge, no work has investigated static ICIC mechanisms applied to the ePDCCH.

Thus, several ICIC strategies based on Soft Frequency Reuse (SFR) [14] are investigated as alternatives to protect the ePDCCH in the context of realistic/irregular macrocellular deployments. Two different multiobjective optimization frameworks are introduced and analyzed. The proposed schemes adjust the operational parameters of SFR and the amount of resources allocated to the ePDCCH in order to optimize several performance metrics such as spectral efficiency, cell edge performance, average consumption of eCCEs, amount of control resources and energy requirements. Therefore, the study presented herein is unique in the sense that it:

- Introduces several effective SFR-based optimization frameworks for the ePDCCH. In fact, not only the performance of this channel is studied, the work also analyses the impact on the capacity of data channels. As a consequence, interesting tradeoffs and design insights are identified.
- Provides means, due to its multiobjective nature, to obtain several network configurations instead of one single solution. This feature is important, because it allows mobile operators to select different configurations according to time-varying network conditions such as load and/or traffic patterns.

The rest of the paper is organized as follows: the next section introduces the system model and provides a brief introduction to the structure of the ePDCCH and the operation of SFR. Section III describes the multiobjective optimization framework and proposed schemes. Finally, the paper is closed with the analysis of numerical results and conclusions in Sections IV and V, respectively.

II. BACKGROUND

A. System Model

This study considers the downlink of a LTE-based cellular network. The system bandwidth B_{SYS} is composed of N_{SC} subcarriers grouped in N_{PRB} Physical Resource Blocks (PRBs). In LTE/LTE-A, a PRB is the minimum allocable resource unit in frequency domain. It is composed of 12 contiguous subcarriers each of them spaced 15 kHz. In time domain, the Transmission Time Interval (TTI) is 1 ms and it contains 14 OFDM symbols. The first 3 symbols are devoted to the PDCCH as it is illustrated in Figure 1. The total available power per cell is $P_{\text{max}}^{\text{Cell}}$. The conclusions obtained in this study are independent of the value of N_{PRB} and hence, more or less PRBs would just shift absolute values. The cellular network, composed of L trisectorial cells, provides service to a coverage area divided in A small area elements (pixels). Given

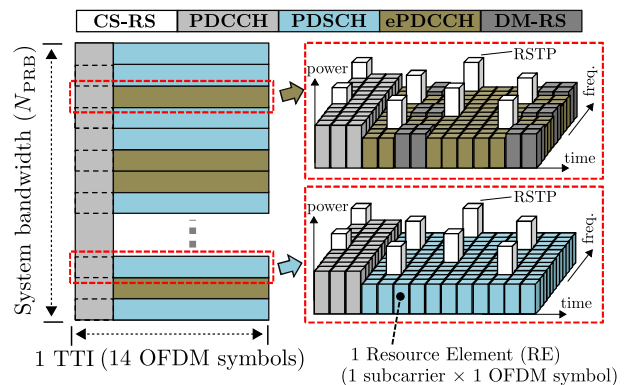


Fig. 1. Structure of the PDCCH and ePDCCH in LTE/LTE-A.

the small granularity used in this study, it is reasonable to assume that within each pixel the average received power and hence, average SINR are constant. Average SINR values \bar{S} are computed based on the average Reference Signals Received Power (RSRP). In LTE and LTE-A, *cell-specific* Reference Signals (CS-RS) are embedded into the system bandwidth to allow for channel estimation, synchronization and cell selection procedures [10]. Due to their importance, CS-RSs are the highest powered components within the downlink signal and they are transmitted with constant power within each cell as it is shown in Figure 1. Thus, the vector $\mathbf{p}_{\text{RSTP}} \in \mathbb{R}^L$ represents the Reference Signals Transmit Power (RSTP) of each cell. The matrix $\mathbf{R}_{\text{RSRP}} \in \mathbb{R}^{A \times L}$ corresponds to the average RSRP at each pixel with respect to each transmitter and it is obtained according to:

$$\mathbf{R}_{\text{RSRP}} = \mathbf{G} \cdot \text{diag}(\mathbf{p}_{\text{RSTP}}) \quad (1)$$

The matrix $\mathbf{G} \in \mathbb{R}^{A \times L}$ contains the Long Term Channel Gain (LTCG) of each pixel with respect to each transmitter. LTCG includes propagation losses, large scale fading and antenna gains. The pixel a (a^{th} row in \mathbf{R}_{RSRP}) is served by the cell l^* from which it receives the highest RSRP, thus:

$$l^* = \underset{l \in \{1, 2, \dots, L\}}{\text{argmax}} \mathbf{R}_{\text{RSRP}}(a, l) \quad (2)$$

Therefore, the binary matrices $\mathbf{S}, \mathbf{S}^c \in \{0, 1\}^{A \times L}$ indicate the coverage of each cell. If a is served by l^* , then $\mathbf{S}(a, l^*) = 1$ and the rest of the a^{th} row is 0. \mathbf{S}^c is the binary complement of \mathbf{S} . It is assumed, without loss of generality, that the power allocated to RSs is the same for all cells and hence, the cell coverage pattern depends on local propagation conditions.

B. Description of the ePDCCH

As it was indicated previously, in order to allow frequency domain ICIC, the ePDCCH is based on FDM as it is illustrated in Figure 1. Note that additional Demodulation Reference Signals (DM-RS) are inserted within the ePDCCH to allow for user-specific beamforming and spatial diversity. Thus, each serving cell can configure a User Equipment (UE) with one or more ePDCCH PRB sets, i.e., a set of contiguous PRBs devoted to allocate the ePDCCH. This user-specific allocation

is transmitted to UE by means of higher layers signaling. The exact position and amount of resources devoted to the ePDCCH can be changed dynamically and it depends on aspects such as system bandwidth, required control capacity and location of the ePDCCH in neighbor cells. Details about the resource allocation control mechanism for the ePDCCH in LTE-A, i.e., how to localize and index the eCCEs within the PRBs carrying the ePDCCH, can be found in [10].

The information transmitted over the ePDCCH includes downlink (and uplink) scheduling grants, power control commands and data required to decode and demodulate OFDM symbols in the downlink (encode and modulate in the uplink) [10]. Given the importance of such information, a target Block Error Rate (BLER) of 1% is pursued for the ePDCCH. Therefore, different ALs in which one or more eCCEs can be grouped have been defined. In this manner, several coding rates provide the required reliability. For a given UE, the selection of the appropriate AL depends on the reported SINR for the subband in which its ePDCCH is allocated. Thus, a user i is assigned with the AL x if its SINR in the subband carrying the ePDCCH is greater than the target SINR of that AL for a BLER of 1% S_{TH}^T . In this study, the focus is precisely on improving the radio quality (SINR) of the ePDCCH by means of SFR, a static ICIC technique described in the next subsection. Other degrees of freedom to enhance the performance of the ePDCCH are dynamic control resource allocation schemes and efficient design of users' search space; examples of these approaches include [8] and [13], respectively.

C. Soft Frequency Reuse

Broadly speaking, the main goal of any ICIC strategy is to enhance the radio channel quality of cell edge users, a well known issue in OFDMA-based cellular technologies such as LTE/LTE-A [15]. As such, SFR accomplishes this target by classifying users in Exteriors (\mathcal{E}) or Interiors (\mathcal{I}) according to their average channel quality (based on CS-RSs and expressed in terms of SINR) and then, applying different power levels to each group in order to reduce the amount of Intercell Interference (ICI) received by cell edge users, thus increasing their SINR. The operation of SFR is illustrated in Figure 2. In order to accomplish such target, a classification threshold S_{TH} must be defined either globally in the network or locally at each cell. This figure has a great impact on the performance of SFR (see [16] and [17]) as it determines the amount of users in each class. Similarly, the bandwidth and power allocated to each group is controlled by means of the parameters β and α respectively. Although SFR proved its effectiveness as an ICIC technique in the context of OFDMA technologies ([18] and [19] are representative examples) its usage was mainly focused on data channels due to the rigid structure of the PDCCH (time-multiplexed). However, as it was introduced previously, the flexible design (based on FDM) of the ePDCCH in LTE-A opens new possibilities from the perspective of ICIC; SFR is certainly an interesting option that is investigated in this paper.

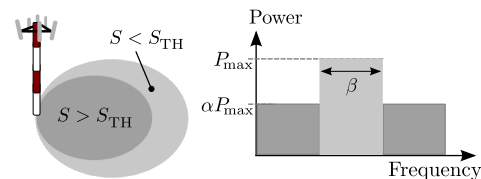


Fig. 2. Operational principle of SFR.

III. RESEARCH FRAMEWORK

A. Multiobjective Problem Formulation

This work investigates the advantages of applying SFR to control channels in LTE-A. However, it is well known that the enhancements in terms of cell edge performance achieved by ICIC techniques are usually obtained at expenses of spectral efficiency losses [16]. For this reason, it is desirable to have a complete picture of the tradeoff existing among conflicting criteria such as spectral efficiency, cell edge performance, energy consumption, etc. Moreover, the problem studied herein adds another interesting perspective: the impact of allocating resources (normally employed for data) to control channels on the overall system performance. Therefore, in order to provide such *visibility*, the performance assessment is based on the joint optimization of the following metrics:

- 1) Maximization of the **average cell capacity** (f_1 [Mbps]): A metric proportional to the system spectral efficiency.
- 2) Maximization of the **capacity of the worst 5% of the coverage area** (f_2 [Mbps]): This indicator indicates the capacity associated to cell edge areas and hence, it is a measure of cell edge performance.
- 3) Minimization of the **average eCCE consumption** (f_3 [eCCE]): This metric reflects the impact of ICI on the radio quality associated to the ePDCCH. It indicates the average consumption of eCCEs per cell.
- 4) Minimization of the **worst eCCE consumption** (f_4 [eCCE]): It corresponds to the average eCCE consumption in the worst cell of the system, i.e., the most interfered cell.
- 5) Maximization of **ePDCCH resources** (f_5 [PRB]): This metric quantifies how many resources are devoted to the ePDCCH. Thus, the maximization of this metric implies more capacity for the control channels. However, it is worth saying that this objective is in conflict with the capacity associated to data channels f_1 .
- 6) Minimization of the **normalized energy consumption** (f_6 [·]): Indicates the energy consumption in the system.

Thus, in order to achieve simultaneous optimization of the previous conflicting objectives, the problem under consideration, i.e., optimization of SFR for the ePDCCH, has been addressed as a multiobjective optimization task. Such problem has been formulated as follows:

$$\begin{aligned} & \text{minimize } \mathbf{f}(\mathbf{x}) \\ & \text{subject to: } \mathbf{x}(l) = x^l \in [x_{\min}^l, x_{\max}^l] \quad \forall l \quad (3) \\ & \mathbf{f}(\mathbf{x}) = [-f_1(\mathbf{x}) \quad -f_2(\mathbf{x}) \quad f_3(\mathbf{x}) \quad f_4(\mathbf{x}) \quad -f_5(\mathbf{x}) \quad f_6(\mathbf{x})] \quad (4) \end{aligned}$$

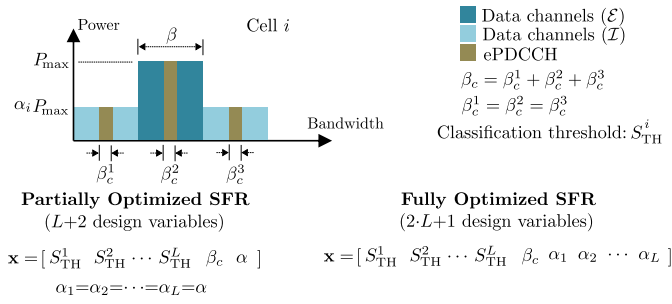


Fig. 3. SFR-based optimization models.

The vectors \mathbf{x} and \mathbf{f} contain the optimization (design) variables and objective function values respectively. The parameters x_{\min}^l and x_{\max}^l are the bounds of the l^{th} design variable. Thus, in order to provide a flexible framework, the optimization of these performance indicators is done by tuning the operational parameters of SFR: α , and S_{TH} (see Figure 2). Two different optimization models are proposed: *Partially Optimized SFR* (POS) and *Fully Optimized SFR* (FOS). Both models are described in the following points:

- 1) **Partially Optimized SFR (POS):** In this scheme, there are L local design variables (classification thresholds) optimized at cell level plus 2 additional network-wide design variables (β_c and α) that are applied globally in the network, i.e., the same value for all cells. The reason for selecting classification threshold S_{TH}^i as local design variables is twofold: first, the performance of SFR is highly sensitive to this parameter with the advantage that varying this parameter locally has no effect on neighbor cells (for a common value of α) and, second, its usage was demonstrated to be effective in SFR optimization for realistic/irregular deployments [20]. In [20], a multiobjective approach is also employed; however it is focussed exclusively on data channels. The parameters β_c and α determine how many resources are devoted to the ePDCCCH and the power ratio between exterior and interior users respectively. As it can be seen in Figure 3, the resources allocated to the ePDCCCH (controlled by β_c) are distributed between the bandwidth portions of each class of user (\mathcal{E} and \mathcal{I}). The bandwidth sharing coefficient β is kept as an input and its value is set to the maximum avoiding overlapping between cell edge subbands, thus $\beta = 1/3$. Thus, the optimization framework employed by this model corresponds to the following mapping: $\mathbf{x} \in \mathbb{R}^{L+2} \rightarrow \mathbf{f} \in \mathbb{R}^6$. The design target of this scheme is achieving a competitive optimization level while keeping the computational complexity as low as possible; that was the reason why in this model α is defined as a network-wide design variable.
- 2) **Fully Optimized SFR (FOS):** This scheme is similar to the previous scheme with the only difference that the power ratio α is optimized locally at each cell in order to attain a higher optimization level although at expense of

Function PreliminaryComp(\cdot)

```

input :  $\mathbf{G}, \mathbf{S}, \mathbf{S}^c, \Psi'_j, \eta, \mathbf{v}_\varphi, \text{PRSTP}$ 
output:  $\mathbf{G}_j, \mathbf{S}_j, \mathbf{S}_j^c, \Psi'_j$ 
// STEP 1: Average SINR (based on CS-RS);
1  $\Psi' = [(\mathbf{S} \odot \mathbf{G}) \cdot \text{PRSTP}] \oslash [[(\mathbf{S}^c \odot \mathbf{G}) \cdot \text{PRSTP}] \oplus \eta]$ ;
// STEP 2: Azimuth classification;
2  $\mathbf{t} \leftarrow \text{AzimuthClass}(\mathbf{v}_\varphi, \mathbf{S})$ ;
// STEP 3: Segmentation;
3 for each  $j \in \mathcal{J}$  do
4    $\{\mathbf{G}_j, \mathbf{S}_j, \mathbf{S}_j^c, \Psi'_j\} \leftarrow \text{Segmentation}(\mathbf{t}, j, \mathbf{G}, \mathbf{S}, \mathbf{S}^c, \Psi')$ ;
5 end
    
```

 Fig. 4. Preliminary computations required for evaluating the objective functions: $f_i, i = 1, 2, \dots, 6$.

additional computational cost. This model corresponds to the following mapping: $\mathbf{x} \in \mathbb{R}^{(2L)+1} \rightarrow \mathbf{f} \in \mathbb{R}^6$

B. Evaluation of Objective Functions

In order to evaluate the objective functions, a preliminary set of computations need to be performed as indicated in Figure 4. Therefore, the objective functions are evaluated by means of the pseudo-code shown in Figure 5. Both pseudo-codes are explained in the following points. Note that the optimization model POS is indeed a particular case of the scheme FOS, when $\alpha_1 = \alpha_2 = \dots = \alpha_L = \alpha$. Thus, the process of evaluating the objective function values is described for the most general case, i.e., the model FOS.

- **PreliminaryComp(\cdot):** The first step (line 1) corresponds to the computation of average SINR values based on RSRP. These figures are used to classify the pixels as \mathcal{E} or \mathcal{I} . Note that \odot, \oslash and \oplus indicate Hadamard (point-wise) operations and η corresponds to the noise power. Then, Function **AzimuthClass(\cdot)** classifies cells according to their azimuth φ (stored in $\mathbf{v}_\varphi \in \mathbb{R}^L$) as follows:

$$j = \begin{cases} 0 & 0^\circ \leq \varphi < 120^\circ \\ 1 & 120^\circ \leq \varphi < 240^\circ \\ 2 & 240^\circ \leq \varphi < 360^\circ \end{cases} \quad (5)$$

Pixels are also classified according to the type of serving cell (see (2)). Thus, cells and pixels belong to one of the sets \mathcal{A}_j with $j \in \mathcal{J} = \{0, 1, 2\}$. This classification is stored in the vector $\mathbf{t} \in \mathbb{N}^A$, where each element (representing one pixel) indicates the type of serving cell it belongs to. Next, Function **Segmentation(\cdot)** (line 4) pulls out from the matrices $\mathbf{G}, \mathbf{S}, \mathbf{S}^c$ and Ψ' the rows whose corresponding value in the vector \mathbf{t} is equal to $j, \forall j \in \mathcal{J}$. In other words, once instructions 3-5 are executed, each one of these matrices is segmented in $|\mathcal{J}|$ submatrices ($\mathbf{S}_j, \mathbf{S}_j^c, \mathbf{G}_j$ and Ψ'_j) each of them having L columns, but a different number of rows and so:

$$\mathbf{S}_j, \mathbf{S}_j^c, \mathbf{G}_j, \Psi'_j \in \mathbb{R}^{|\mathcal{A}_j| \times L} \quad \forall j \in \mathcal{J}$$

- **ObjFunc(\cdot):** Once Function **PreliminaryComp(\cdot)** is executed, and having fixed $\mathbf{G}_j, \mathbf{S}_j, \mathbf{S}_j^c, \Psi'_j \forall j \in \mathcal{J}$, the

Function ObjFunc(x)

```

input :  $\mathbf{x}$ ,  $\mathbf{G}_j$ ,  $\mathbf{S}_j$ ,  $\mathbf{S}_j^c$ ,  $\Psi_j'$ ,
output:  $\mathbf{f}$ 
// Classification thresholds;
1  $\mathbf{s}_{TH} \leftarrow \mathbf{x}(1:L)$ ;
// ePDCCCH bandwidth;
2  $\beta_c \leftarrow \mathbf{x}(L+1)$ ;
// Power ratios:  $\mathbf{v}_\alpha(l) = \alpha_l$ ;
3  $\mathbf{v}_\alpha \leftarrow \mathbf{x}(L+2:2 \cdot L+1)$ ;
// Classification of pixels:  $\mathcal{E}$  or  $\mathcal{I}$ ;
4 for each  $j \in \mathcal{J}$  do
5    $\mathbf{C}_j \leftarrow \text{Class}(\mathbf{S}_j, \mathbf{s}_{TH}, \Psi_j')$ ;
6 end
// Relative coverage per cell;
7  $\Phi \leftarrow \text{RelCov}(\mathbf{S}_1, \dots, \mathbf{S}_{|\mathcal{J}|}, \mathbf{C}_1, \dots, \mathbf{C}_{|\mathcal{J}|})$ ;
// Power matrices;
8  $\mathbf{P}_{ser} = \begin{bmatrix} P_{max} & P_{max} & \dots & P_{max} \\ \alpha_1 P_{max} & \alpha_2 P_{max} & \dots & \alpha_L P_{max} \end{bmatrix}^T$ ;
9 for each  $s = 0 : ((L/3) - 1)$  do
10    $\mathbf{P}_{int}^{base}(s) = \begin{bmatrix} P_{max} & \alpha_{(3s)} P_{max} & \alpha_{(3s)} P_{max} \\ \alpha_{(3s+1)} P_{max} & P_{max} & P_{max} \\ P_{max} & \alpha_{(3s+1)} P_{max} & \alpha_{(3s+1)} P_{max} \\ \alpha_{(3s+2)} P_{max} & \alpha_{(3s+2)} P_{max} & P_{max} \\ \alpha_{(3s+2)} P_{max} & P_{max} & \alpha_{(3s+2)} P_{max} \end{bmatrix}^T$ ;
11 end
12  $\mathbf{P}_{int} = [\mathbf{P}_{int}^{base}(0)^T \quad \mathbf{P}_{int}^{base}(1)^T \quad \dots \quad \mathbf{P}_{int}^{base}((L/3) - 1)^T]^T$ ;
// Bandwidth matrix;
13  $\mathbf{B} \leftarrow \mathbf{B}_{SYS} \cdot [(1/3 - (1/3 \cdot \beta_c)) \quad ((2/3) - (2/3 \cdot \beta_c))]$ ;
// Reset accumulators;
14  $f_1 \leftarrow 0$ ,  $f_2 \leftarrow 0$ ,  $\hat{\mathbf{r}} \leftarrow []$ ;
// Resize  $\mathbf{p}_\gamma$  (pointers to per-cell SINR values);
15  $\text{Resize}(\mathbf{p}_\gamma, (2 \cdot L))$ ;
// For each group of pixels (for each  $j \in \mathcal{J}$ );
16 for each  $j \in \mathcal{J}$  do
17    $\hat{\mathbf{P}}_{int} \leftarrow \mathbf{P}_{int}(:, 2j : 2j + 1)$ ;
18    $\Delta_j \leftarrow [(\mathbf{S}_j \odot \mathbf{G}_j) \cdot \mathbf{P}_{ser}] \odot [(\mathbf{S}_j^c \odot \mathbf{G}_j) \cdot \hat{\mathbf{P}}_{int}] \oplus \eta$ ;
19    $\text{UpdatePerCellSINR}(\mathbf{p}_\gamma, \Delta_j)$ ;
20    $\Psi_j \leftarrow \Delta_j \odot \mathbf{C}_j$ ;
21    $\Lambda_j \leftarrow \text{LinkPer}(\Psi_j)$ ;
22    $f_1 \leftarrow f_1 + [\mathbf{B} \cdot [(\Lambda_j^T \cdot \mathbf{S}_j) \odot \Phi]] \cdot \mathbf{1}$ ;
23    $\mathbf{r} \leftarrow [(\mathbf{S}_j \cdot (\Phi^T \cdot \text{diag}(\mathbf{B}))) \odot \Lambda_j] \cdot \mathbf{1}$ ;
24    $\hat{\mathbf{r}} \leftarrow [\hat{\mathbf{r}} \quad \mathbf{r}^T]$ ;
25 end
26  $f_2 \leftarrow \text{CapPerc}(\hat{\mathbf{r}})$ ;
27  $f_5 \leftarrow \beta_c \cdot N_{PRB}$ ;
28  $f_6 \leftarrow 1 - ((2/3) \cdot (1 - \alpha))$ ;
// For each cell  $l$ ;
29 for each  $l = 1 : L$  do
30    $f_\mathcal{E} \leftarrow \text{CDF}(\mathbf{p}_\gamma(2 \cdot l - 1))$ ;  $f_\mathcal{I} \leftarrow \text{CDF}(\mathbf{p}_\gamma(2 \cdot l + 1))$ ;
31    $p_\mathcal{E}^0 \leftarrow (1 - f_\mathcal{E}(S_0^0))$ ;  $p_\mathcal{E}^1 \leftarrow (f_\mathcal{E}(S_0^0) - f_\mathcal{E}(S_1^0))$ ;
32    $p_\mathcal{E}^2 \leftarrow (f_\mathcal{E}(S_1^0) - f_\mathcal{E}(S_2^0))$ ;  $p_\mathcal{E}^3 \leftarrow f_\mathcal{E}(S_2^0)$ ;
33    $p_\mathcal{I}^0 \leftarrow (1 - f_\mathcal{I}(S_0^1))$ ;  $p_\mathcal{I}^1 \leftarrow (f_\mathcal{I}(S_0^1) - f_\mathcal{I}(S_1^1))$ ;
34    $p_\mathcal{I}^2 \leftarrow (f_\mathcal{I}(S_1^1) - f_\mathcal{I}(S_2^1))$ ;  $p_\mathcal{I}^3 \leftarrow f_\mathcal{I}(S_2^1)$ ;
35    $\Gamma_\mathcal{E}^l \leftarrow (p_\mathcal{E}^0 \cdot \text{AL}_0) + (p_\mathcal{E}^1 \cdot \text{AL}_1) + (p_\mathcal{E}^2 \cdot \text{AL}_2) + (p_\mathcal{E}^3 \cdot \text{AL}_3)$ ;
36    $\Gamma_\mathcal{I}^l \leftarrow (p_\mathcal{I}^0 \cdot \text{AL}_0) + (p_\mathcal{I}^1 \cdot \text{AL}_1) + (p_\mathcal{I}^2 \cdot \text{AL}_2) + (p_\mathcal{I}^3 \cdot \text{AL}_3)$ ;
37    $\mu_\mathcal{E} \leftarrow (1/\Phi(0, l))$ ;  $\mu_\mathcal{I} \leftarrow (1/\Phi(1, l))$ ;
38    $\Gamma(l) \leftarrow [(\mu_\mathcal{E}/(\mu_\mathcal{E} + \mu_\mathcal{I})) \cdot \Gamma_\mathcal{E}^l] + [(\mu_\mathcal{I}/(\mu_\mathcal{E} + \mu_\mathcal{I})) \cdot \Gamma_\mathcal{I}^l]$ ;
39 end
40  $f_3 \leftarrow \text{mean}(\Gamma)$ ;
41  $f_4 \leftarrow \text{max}(\Gamma)$ ;
42  $\mathbf{f} \leftarrow [-f_1/L \quad -f_2 \quad f_3 \quad f_4 \quad -f_5 \quad f_6]$ ;

```

Fig. 5. Pseudo code corresponding to the evaluation of the objective functions considered in this study.

vector \mathbf{f} (objective function values) depends exclusively on \mathbf{x} , a potential solution or SFR configuration. First, Function `Class()` (line 5) calculates the binary matrices

$\mathbf{C}_j \in \mathbb{R}^{|\mathcal{A}_j| \times 2} \forall j \in \mathcal{J}$ indicating the class (\mathcal{E} or \mathcal{I}) to which each pixel belongs to. The value '1' in column 0 or 1 indicates the pixel belongs to \mathcal{E} or \mathcal{I} respectively. Next, Function `RelCov()` (line 7) computes the matrix $\Phi \in \mathbb{R}^{2 \times L}$. While the columns of Φ correspond to cells, the rows 0 and 1 are the inverse of the number of pixels classified as \mathcal{E} and \mathcal{I} (at each cell) respectively. As SFR assigns specific portions of the system bandwidth to each group of pixels (\mathcal{E} and \mathcal{I}), Φ is required to guarantee bandwidth proportionality and hence, calculate true average values. Instructions from line 8 to 12 create the matrices corresponding to the particular power allocation specified by \mathbf{x} . In line 13, the bandwidth allocated to each class of users is calculated as a function of β_c . In line 15, a vector of $2 \cdot L$ pointers is created. They point to vectors storing the SINR distribution of each class (\mathcal{E} and \mathcal{I}) at each cell. The loop comprising the lines 16 to 25 determines the capacity in bps associated to each pixel; once this loop is executed, the vector $\hat{\mathbf{r}} \in \mathbb{R}^A$ contains such information. Function `UpdatePerCellSINR()` updates the statistic of the SINR per class/cell by using the SINR values stored in the matrix $\Delta_j \in \mathbb{R}^{|\mathcal{A}_j| \times 2}$. Function `LinkPer()` computes for every single element of $\Psi_j \in \mathbb{R}^{|\mathcal{A}_j| \times 2}$ a non-decreasing function of the SINR. Thus $\text{LinkPer}(z) = \text{Log}_2(1 + z)$ [bps/Hz], i.e., the Shannon bound. Finally, the metrics related to the consumption of eCCEs (f_3 and f_4) are obtained in a per-cell basis by means of the instructions in the loop comprising the lines 29 to 39. To be precise, the Cumulative Density Function (CDF) of each class (\mathcal{E} and \mathcal{I}) at each cell is estimated by means of Function `CDF()` using the information pointed from \mathbf{p}_γ . Note that $\mathbf{p}_\gamma(2 \cdot l - 1)$ and $\mathbf{p}_\gamma(2 \cdot l)$ point to the vectors containing the SINR values of the classes \mathcal{E} and \mathcal{I} (at the l^{th} cell) respectively. Once the CDFs are obtained, the instructions from line 31 to 38 determine the average eCCE consumption at each cell taking into account the relevant information of each AL. To be precise, for the AL x , the number of eCCEs and target SINR are specified by AL_x and S_x^T respectively. Recall that S_x^T represents the target SINR of the AL_x for a BLER of 1%.

C. Multiobjective Evolutionary Optimization

In the light of the previous subsection, where objective functions were defined, it is clear that the *domain* (search space) created by the optimization variables is a n -dimensional space, where $n = L + 2$ and $n = 2 \cdot L + 1$ for POS and FOS respectively. Given that the objective space (or *image* defined by such objectives is not only highly non-linear, non-convex, but also full of discontinuities and local optima [21], traditional optimization approaches such as Simplex [22] can not be employed as they are susceptible to be trapped in local minima. Other techniques such as Sequential Quadratic Programming based methods [23] require convexity (a very strong assumption in this context) to guarantee convergence.

Summarizing, the problem of interest requires of an optimization tool fulfilling the following set of features:

- It must be able to find good solutions by efficiently exploring the search space.
- It should operate efficiently with multiple criteria and a large number of design variables.
- It should not have strong requirements on objective functions such as linearity, convexity, continuity or differentiability.

Multiobjective evolutionary algorithms (MOEAs) [24] fulfill the previous requirements and hence, their usage in this context has been investigated. MOEAs are population-based metaheuristics that simulate the process of natural evolution. In MOEAs, a population of individuals (candidate solutions) is iteratively modified by means of two basic principles: selection and variation. While selection tries to imitate the battle for reproduction among living beings, variation mimics their inherent ability of creating new (better adapted) individuals through recombination and mutation. A well-known MOEA has been selected for this study: The Non-dominated Sorting Genetic Algorithm II (NSGA-II) [25]. The reason is that this algorithm provides means to accomplish desired features such as: elitism, fast convergence and good distribution of solutions. Interested readers are referred to [26] for further details. Finally, recall that multiobjective optimization has an additional advantage: the solution is not only one single configuration but a set of so many Pareto Efficient solutions. A solution \mathbf{x}_1 is preferred to (dominates in the Pareto sense) another solution \mathbf{x}_2 , ($\mathbf{x}_1 \succ \mathbf{x}_2$), if \mathbf{x}_1 is better than \mathbf{x}_2 in at least one criterion and no worse with respect to the remaining ones. The set of nondominated solutions \mathcal{X}^* is called Pareto Front.

IV. NUMERICAL RESULTS

In order to perform numerical evaluations, a realistic cellular deployment covering the city of Vienna and its surroundings has been considered. This deployment represents the system model described in Subsection II-A. Actual parameter values are shown in Table I. To be precise, the cellular layout is composed of 60 tri-sectorial cells. The evaluation area corresponds to a urban subarea of $2.75 \times 2.625 \text{ km}^2$. The digital elevation model and cell parameters have been obtained from the MORANS initiative [27]. The propagation model is the COST 231-Walfish-Ikegami. Figure 6 shows the cellular layout and the resulting propagation pattern for one site as reference. In addition, the CDFs of \bar{S} corresponding to the coverage of each cell are also shown. It can be observed how much different those CDFs are. It can be noticed that areas in which the average SINR $\bar{S} < 0 \text{ dB}$ vary from 5 to 70% of the total coverage at different cells. These *differences* are exploited by the proposed framework in order to fit SFR to the scenario under consideration and hence, maximize its benefits.

The list of parameters employed for NSGA-II together with the rest of parameters employed in numerical evaluations are shown in Table I. In general, the performance (convergence) of

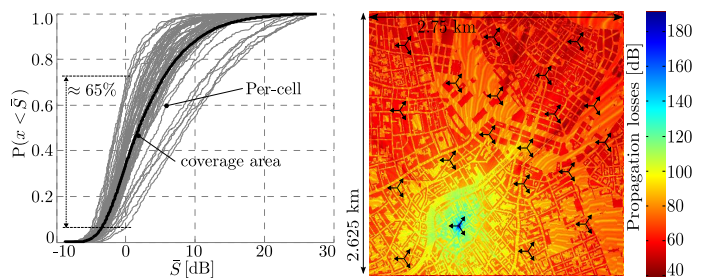


Fig. 6. Realistic deployment used in numerical evaluations. Left: Per-cell and global SINR statistic. Right: one single site propagation losses.

TABLE I
EVALUATION SETTING

Parameter	Value
NSGA-II: Population size	300
NSGA-II: Max number of generations	3000
NSGA-II: Crossover probability	1.0
NSGA-II: Mutation probability	$1/(L+1)$
NSGA-II: Design variables type	Binary coded
System model: [$A \ L \ \eta$]	[288750 60 -125 dBm/15kHz]
System model: Pixel resolution	$5 \times 5 \text{ m}^2$
System model: [$B_{\text{SYS}} \ N_{\text{SC}} \ N_{\text{PRB}}$]	[5.40 MHz 360 30]
System model: [$P_{\text{Cell}}^{\text{max}} \ \beta$]	[43.0 dBm 1/3]
System model: [$P_{\text{max}} \ \text{RSTP}$]	[17.4 18.5] dBm/15kHz
System model: [$AL_0 \ AL_1 \ AL_2 \ AL_3$]	[1 2 4 8]
System model: [$S_0^T \ S_1^T \ S_2^T \ S_3^T$]	[9.25 2.50 -0.50 -2.50] dB [28]
MO problem: [$\beta_{c,\text{min}} \ \beta_{c,\text{max}}$]	[0.10 0.30]
MO problem: [$\alpha_{l,\text{min}} \ \alpha_{l,\text{max}}$]	[0.15 0.60]
MO problem: [$S_{\text{TH},\text{min}}^l \ S_{\text{TH},\text{max}}^l$]	[-3.00 6.00] dB

NSGA-II depends on its operational parameters. The following points are practical calibration guidelines:

- **Population size:** It is widely accepted that populations larger than 100 individuals only provide marginal gains and the same global convergence is obtained [29]. However, in some cases such as the problem herein, larger populations will have the benefit of getting more solutions or network settings at expenses of computational cost.
- **Termination criterion:** The execution of NSGA-II finishes when the improvement of each objective function is less than 0.001% after a block of 40 generations.
- **Genetic operators:** Crossover and mutation are important in genetic algorithms to preserve elitism and achieve good diversity respectively. Crossover and mutation rates (probabilities) follow the recommendations given in [25].

For comparison, several benchmarks have been considered. These references include the important case of Full Frequency Reuse (FFR) and baseline designs of SFR according to the bandwidth proportionality criterion (see [15] and [30]), i.e., schemes in which optimization is not available and hence, the parameters α , β and S_{TH} are selected according to the SINR statistic (observed in the whole coverage area) and applied globally. The configurations of these benchmarks together with their corresponding objective function values are shown in

TABLE II
 BENCHMARKS

Ref	Type	S_{TH} [dB]	α	β	β_c	f_1 [Mbps]	f_2 [Mbps]	f_3 [eCCE]	f_4 [eCCE]	f_5 [PRB]	f_6 [·]
x_{FFR}^1	FFR	N/A	N/A	N/A	0.10	8.38	7.54	4.25	6.26	3.00	1.00
x_{FFR}^2	FFR	N/A	N/A	N/A	0.20	7.45	6.70	4.25	6.26	6.00	1.00
x_{FFR}^3	FFR	N/A	N/A	N/A	0.30	6.52	5.87	4.25	6.26	9.00	1.00
x_{SFR}^1	SFR	0.00	0.40	1/3	0.10	7.51	8.11	4.08	5.67	3.00	0.60
x_{SFR}^2	SFR	0.00	0.40	1/3	0.20	6.50	7.03	4.08	5.67	6.00	0.60
x_{SFR}^3	SFR	0.00	0.40	1/3	0.30	5.84	6.31	4.08	5.67	9.00	0.60

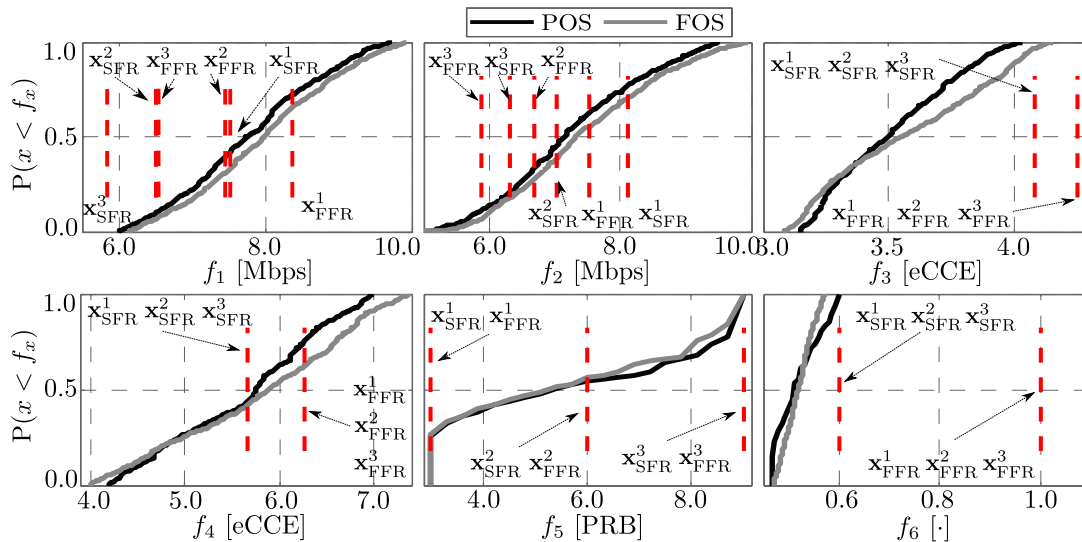


Fig. 7. Overall performance obtained by means of the optimization frameworks POS and FOS.

Table II. The statistic of the different performance metrics corresponding to the sets of nondominated solutions of the models POS and FOS, \mathcal{X}_{POS}^* and \mathcal{X}_{FOS}^* respectively, is shown in Figure 7. In the figure, the performance of the benchmarks is also plotted (in red). These results indicate, on the one hand, that the SFR settings obtained through the proposed schemes are able to offer different tradeoffs among f_1 , f_2 , f_4 and f_5 while, on the other hand, the performance in terms of f_3 and f_6 is always enhanced with respect to the benchmarks. This means that by applying the solutions in the sets \mathcal{X}_{POS}^* and \mathcal{X}_{FOS}^* it is possible to select different tradeoffs among the performance metrics such as spectral efficiency vs. cell edge performance (f_1 vs. f_2) or spectral efficiency vs. resources allocated to control channels (f_4 vs. f_5), but always achieving gains in terms of eCCE and energy consumption (f_3 and f_6). Note that the performance obtained by means of the model FOS is slightly better than the model POS. This is especially noticeable in terms of f_1 and f_2 . Moreover, the smallest values of f_3 and f_4 are also attained through elements in \mathcal{X}_{FOS}^* , which is expected given the higher number of optimization variables used by this model. However, focusing on each benchmark separately, Figure 8 shows the gains that can be achieved with respect to each benchmark and performance metric. Such gains are computed based on the subsets of solutions dominating

each benchmark in the Pareto sense and hence, no loss is expected. The cardinality of these subsets for each model is presented in Table III. Clearly, the proposed frameworks always succeed in finding non-empty sets of SFR configurations outperforming each reference scheme. The gains shown in Figure 8 make evident that significant improvement are obtained with respect to the important case of Full Frequency Reuse. Both subfigures include an example indicating how they must be read. For instance, focusing on Figure 8b and x_{FFR}^2 , it has been obtained that the energy consumption (f_6) can be decreased up to 53% without losses in terms of any other performance metric. The proposed schemes outperform all the benchmarks achieving gains of 20% or more in at least one of the objective functions.

These results confirm the effectiveness of the optimization models presented herein as they are able not only to **achieve effective ICIC for the ePDCCH** (this is evident given the gains in terms of f_3 and f_4) but also to **improve spectral efficiency and cell edge performance** (f_1 and f_2). This is quite interesting if one takes into account that some of the SFR settings found so far, accomplish the previous and, in addition, increase the amount of resources available for the ePDCCH.

In order to provide additional insights on the tradeoff between the performance metrics, 2D profiles are presented

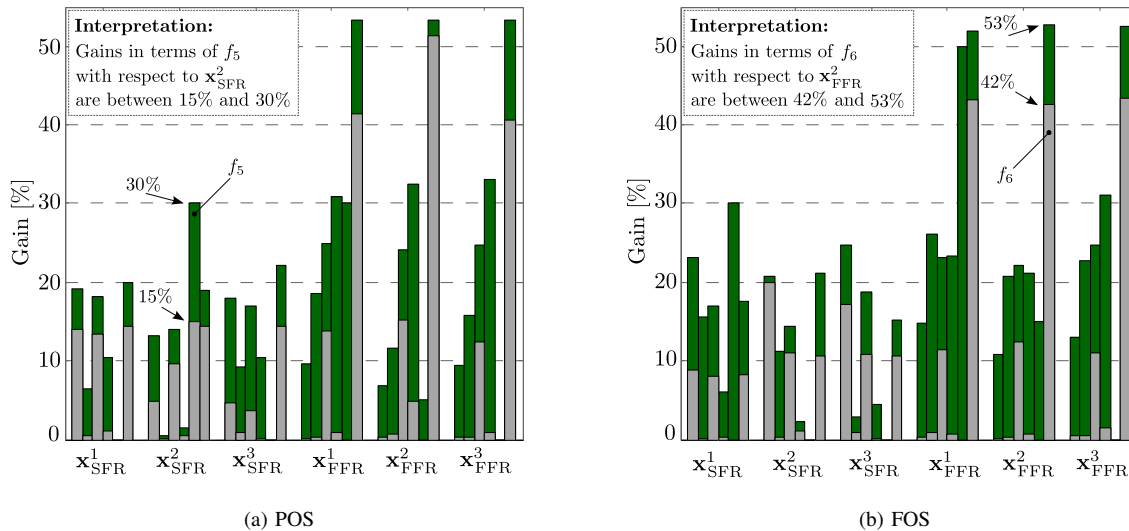


Fig. 8. Gains achieved by means of the proposed optimization models.

in Figure 9. 2D profiles are generated by projecting the Pareto Front onto different planes in order to obtain alternative representations providing better insights about the tradeoff between any pair of objective functions. The figure includes 3 different planes: f_1 - f_2 , f_1 - f_5 and f_3 - f_4 . While in the two first cases, it is notorious the conflicting nature of each pair of metrics, note how the last case, f_3 - f_4 , suggests that SFR settings attaining better average eCCE consumption are also able to minimize the consumption of control resources in the worst cell of the system, which is not evident from the analogy that could be made a priori with f_1 - f_2 . Thus, as a conclusion, while the amount of resources allocated to the ePDCCH f_5 presents a tradeoff with the spectral efficiency f_1 and hence f_2 , the average consumption of control resources is basically linked to the ICIC mechanism employed to protect the ePDCCH. In practice, it will also depend on system load, and in particular, on the amount of low-rate services such as VoIP that tend to heavily load control channels.

Finally, to close the section, Figure 10 illustrates the convergence pattern of both optimization frameworks in terms of the hypervolume of the Pareto front \mathcal{L} [31]. It can be seen that initially the convergence of FOS is slower than POS. This is due to the higher number of design variables that need to be adjusted in FOS. However, after a certain number of generations (approx. 500), FOS features better convergence, explaining so the differences in performance previously found. However, it is worth mentioning that both schemes are valid since there are cases in which the computational cost is a limiting factor, for instance, in very large scale scenarios, and hence a 3% in convergence can be traded by an interesting saving of 26% in processing that can be achieved by means of POS.

 TABLE III
 CARDINALITY OF THE SUBSETS DOMINATING EACH BENCHMARK.

Model	x_{FFR}^1	x_{FFR}^2	x_{FFR}^3	x_{SFR}^1	x_{SFR}^2	x_{SFR}^3
POS	36	3	22	8	2	10
FOS	47	7	29	13	3	10

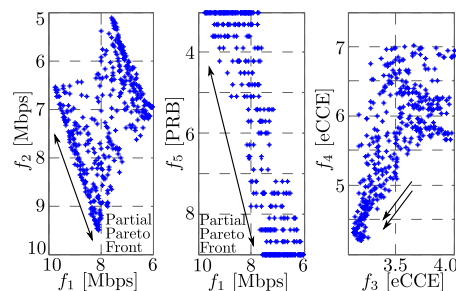


Fig. 9. 2D representations of the resulting Pareto Front: POS model.

V. CONCLUSIONS AND FUTURE WORK

A novel multiobjective algorithm has been proposed for SFR optimization aiming at improving the performance of the ePDCCH in LTE-A networks. The optimization frameworks presented herein have been designed to be applied in realistic/irregular macro/micro cellular deployments, for which only (commonly available) propagation information is required. The proposed schemes succeed in finding good quality SFR settings achieving significant gains with respect to baseline designs and important reference schemes such as full frequency reuse. It was found that, by means of the proposed framework, the overall performance of the ePDCCH can be increased **without penalizing** neither spectral efficiency nor cell edge performance. Indeed, results indicate that the effective intercell interference coordination achieved by the

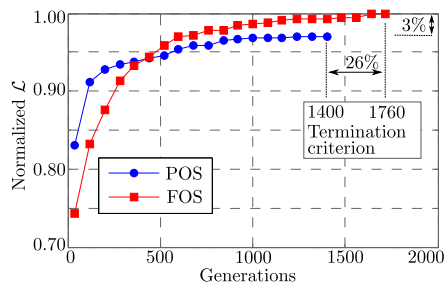


Fig. 10. Convergence pattern of the optimization models: POS and FOS.

proposed schemes results in significant gains in terms of average eCCE consumption (f_3) and transmitted power (f_6). The gains with respect to the important case of full frequency reuse range from 12% to 30% and 11% to 25% for POS and FOS respectively while reducing the transmitted power at least 40% in any of these cases.

Finally, as future research item, adaptive mechanisms able to cope with heterogeneous/irregular traffic distributions both in time and space are going to be investigated. Also, more realistic traffic models (real-time and elastic services) are expected to be included into our framework.

ACKNOWLEDGMENT

This work has been funded through the project TEC2011-27723-C02-01 (Spanish Industry Ministry) and the European Regional Development Fund (ERDF).

REFERENCES

- [1] Mobile web watch 2012, Accenture, 2012, Available online at: www.accenture.com, [retrieved: Feb, 2013].
- [2] S. Sesia, I. Toufik, and M. Baker, *The UMTS Long Term Evolution: From Theory to Practice*, 2nd ed. John Wiley & Sons, 2011.
- [3] Status of the LTE ecosystem, Global mobile Suppliers Association (GSA), 2013, Available online at: www.gsacom.com/news/, [retrieved: Jan, 2013].
- [4] S. Ye, S. Wong, and C. Worrall, "Enhanced physical downlink control channel in LTE advanced release 11," *IEEE Communications Magazine*, vol. 51, no. 2, pp. 82–89, February 2013.
- [5] Group Radio Access Network (GRAN), Technical Specifications: 36.211 (Physical Channels and Modulation), 36.213 (Physical Layer Procedures), 3GPP, 2008, Release 8.
- [6] J. Puttonen, H.-H. Puupponen, K. Aho, T. Henttonen, and M. Moisio, "Impact of control channel limitations on the LTE VoIP capacity," in *Networks (ICN)*, 2010 Ninth Int. Conference on, Apr 2010, Muires, France.
- [7] D. González, M. García-Lozano, S. Ruiz, and J. Olmos, "On the role of downlink control information in the provision of QoS for NRT services in LTE," in *Vehicular Technology Conference (VTC Spring)*, 2012 IEEE 75th, May 2012, pp. 1–5, Yokohama, Japan.
- [8] Y. Yan, A. Li, A. Harada, and H. Kayama, "Enhanced downlink control channel resource allocation algorithm for cross-carrier scheduling in LTE-Advanced carrier aggregation system," in *Vehicular Technology Conference (VTC Spring)*, 2011 IEEE 73rd, May 2011, pp. 1–5, Budapest, Hungary.
- [9] Y. Zhu, A. Li, and A. Harada, "Novel method to improve control channel reliability in LTE-Advanced heterogeneous network," in *Vehicular Technology Conference (VTC Fall)*, 2012 IEEE 76th, Sept. 2012, pp. 1–5, Québec City, Canada.
- [10] Group Radio Access Network (GRAN), Technical Specifications: 36.211 (Physical Channels and Modulation), 36.213 (Physical Layer Procedures), 3GPP, 2012, Release 11.
- [11] Group Radio Access Network, TS 22.146: Multimedia Broadcast/Multicast Service, 3GPP, Jun 2008, v8.4.0.
- [12] M. Einhaus, C. Wengerter, J. Ohlhorst, and S. Feng, "Performance study of an enhanced downlink control channel design for LTE," in *Vehicular Technology Conference (VTC Spring)*, 2012 IEEE 75th, 2012, pp. 1–5, Yokohama, Japan.
- [13] W. Yi, Z. Hua, and W. Jianming, "The search space design for enhanced downlink control channel in LTE-Advanced system," in *Wireless Communications and Mobile Computing Conference (IWCMC)*, 2012 8th International, 2012, pp. 322–326, Venice, Italy.
- [14] Huawei, R1-050507: Soft Frequency Reuse Scheme for UTRAN LTE, 3GPP, May 2005, TSG RAN WG1 Meeting #41: Athens, Greece.
- [15] D. González, M. García-Lozano, S. Ruiz, and J. Olmos, "On the need for dynamic downlink intercell interference coordination for realistic LTE deployments," *Wireless Communications and Mobile Computing*, pp. 1–26, 2012, John Wiley & Sons, Ltd. DOI: 10.1002/wcm.2191.
- [16] T. Novlan, R. Ganti, A. Ghosh, and J. Andrews, "Analytical Evaluation of Fractional Frequency Reuse for OFDMA Cellular Networks," *Wireless Communications*, *IEEE Transactions on*, no. 99, pp. 1–12, Sep 2011.
- [17] D. González G., M. García-Lozano, S. Ruiz, and J. Olmos, "An analytical view of static intercell interference coordination techniques in OFDMA networks," in *IEEE Wireless Communications and Networking Conference (WCNC)*, Apr 2012, pp. 1–6, Paris, France.
- [18] D. Jia, G. Wu, S. Li, G. Li, and X. Zhu, "Dynamic soft-frequency reuse with inter-cell coordination in OFDMA networks," in *Computer Communications and Networks (ICCCN)*, Proceedings of 20th International Conference on, Aug 2011, pp. 1–6, Hawaii, United States.
- [19] L. Chen and D. Yuan, "Soft Frequency Reuse in Large Networks with Irregular Cell Pattern: How Much Gain to Expect?" in *Personal, Indoor and Mobile Radio Communications (PIMRC)*, IEEE 20th International Symposium on, 2009, pp. 1467–1471, Tokyo, Japan.
- [20] D. Gonzalez G., M. Garcia-Lozano, S. Ruiz Boque, and D. Lee, "Optimization of soft frequency reuse for irregular LTE macrocellular networks," *Wireless Communications*, *IEEE Transactions on*, pp. 1–14, 2013.
- [21] T. Weise, *Global Optimization Algorithms - Theory and Application*, 2nd ed. Self-Published, Jun. 26, 2009, available online at <http://www.it-weise.de/>, [retrieved: Mar, 2013].
- [22] D. Gale, "Linear programming and the Simplex method," *Notices of the AMS*, vol. 54, no. 3, pp. 364–369, March 2007.
- [23] Gill, P. E. and Wong, E., "Sequential Quadratic Programming Methods," Department of Mathematics, University of California, San Diego, La Jolla, CA, Tech. Rep. NA-10-03, Aug 2010.
- [24] C. A. Coello, G. B. Lamont, and D. A. Van Veldhuizen, *Evolutionary Algorithms for Solving Multi-Objective Problems*, 2nd ed. Springer: Genetic and Evolutionary Computation Series, 2007.
- [25] K. Deb, A. Pratap, S. Agarwal, and T. Meyarivan, "A fast and elitist multiobjective genetic algorithm: NSGA-II," *Evolutionary Computation*, *IEEE Transactions on*, vol. 6, no. 2, pp. 182–197, Apr 2002.
- [26] J. Jürgen Branke, K. Deb, K. Miettinen, and R. E. Slowiński, *Multiobjective Optimization: Interactive and Evolutionary Approaches*. Springer: Lecture Notes in Comp. Science 5252, 470p, 2008.
- [27] Verdone, R. *et al*, "MORANS White Paper - Update," COST 273, Greece, Tech. Rep. available as TD(04)062, Jan. 26–28, 2004.
- [28] HTC, R1-122331: eREG and eCCE Definitions for ePDCCH, 3GPP, May 2012, TSG RAN WG1 Meeting #69: Prague, Czech Republic.
- [29] J. C. Spall, *Introduction to stochastic search and optimization*, 1st ed. Wiley-Interscience, 2003.
- [30] D. González G., M. García-Lozano, S. Ruiz, and J. Olmos, "Static Inter-Cell Interference Coordination Techniques for LTE Networks: A Fair Performance Assessment," *Lecture Notes in Computer Science*, vol. 6235, no. 68, pp. 211–222, Sep 2010, Springer Berlin / Heidelberg.
- [31] E. Zitzler and L. Thiele, "Multiobjective optimization using evolutionary algorithms - A comparative case study," in *Parallel Problem Solving from Nature V*. Springer, 1998, pp. 292–301.